Simultaneous Trajectory Tracking Control and Online Mass Estimation for a Regolith Excavating Robot via Integral Concurrent Learning

Max L. Greene*,
University of Florida, Gainesville, Florida 32611
Michael DuPuis†, Joe Cloud‡,
Kennedy Space Center, Cape Canaveral, Florida 32899
and
Warren E. Dixon§
University of Florida, Gainesville, Florida 32611

An adaptive controller is developed for a regolith excavation robot to determine the mass of excavated material and to account for the effects of gravity and friction while on the surface of other celestial bodies. A data-based integral concurrent learning (ICL) parameter update law accounts for and estimates the unknown mass, gravity, and friction parameters. A Lyapunov-based analysis proves that the trajectory tracking error and the parameter estimate errors exponentially converge to zero. An estimation of the mass of regolith excavated by the robot is calculated from the estimated parameters. A simulation study is performed to show the performance of the developed technique. Simulation results show that for 3 kilograms of excavated material, the mass estimate has an error of 4.9 grams.

I. Introduction

The Regolith Advanced Surface Systems Operations Robot (RASSOR) is designed to manipulate, excavate, acquire, haul, and dump regolith (e.g., Lunar soil) on the surface of other celestial bodies (e.g., Earth's moon or Mars).[1,2] As depicted in Figure 1, RASSOR has two sets of lifting arms that each hold a bucket drum excavator. A motor is located on the base of the mobile robot and actuates the lifting arm. Another motor is located at the end of the lifting arm and actuates the bucket drum excavator.

Before excavation, the bucket drum excavator's center of mass is located at its centerline. During excavation, regolith is collected and stored in the bucket drum excavator. After excavation, gravitational forces cause regolith to collect at the lowest point of the bucket drum excavator. Due to the distribution of regolith, the combined center of mass of the bucket drum excavator and regolith changes.

RASSOR has the ability to excavate 2.7 metric tons of regolith per day;[2] however, it does not have sensors that can directly measure the mass of regolith that it has excavated (e.g., a digital scale or sensor). Conventional methods, such as measuring the torque required to lift the bucket drum excavator with and without regolith, could be used to calculate the mass of the excavated material. The motor torque is directly proportional to the current supplied to the motor. Since this method relies on one current sensor, any noise, bias, or drift in the sensor will be directly reflected in the mass estimate. RASSOR can be modeled as an Euler-Lagrange dynamic system with constant, unknown coefficients that can be linearly parameterized. If the unknown parameters in the dynamics are perfectly estimated, then the mass of the excavated regolith can

*Graduate Research Assistant, Department of Mechanical and Aerospace Engineering; maxgreene12@ufl.edu.
†Principal Investigator - Robotics and Autonomous Systems, National Aeronautics and Space Administration (NASA) Kennedy Space Center; michael.a.dupuis@nasa.gov.
‡Engineering Trainee, Swamp Works Laboratory, NASA Kennedy Space Center; joe.cloud@nasa.gov.
§Professor, Department of Mechanical and Aerospace Engineering; wdixon@ufl.edu.

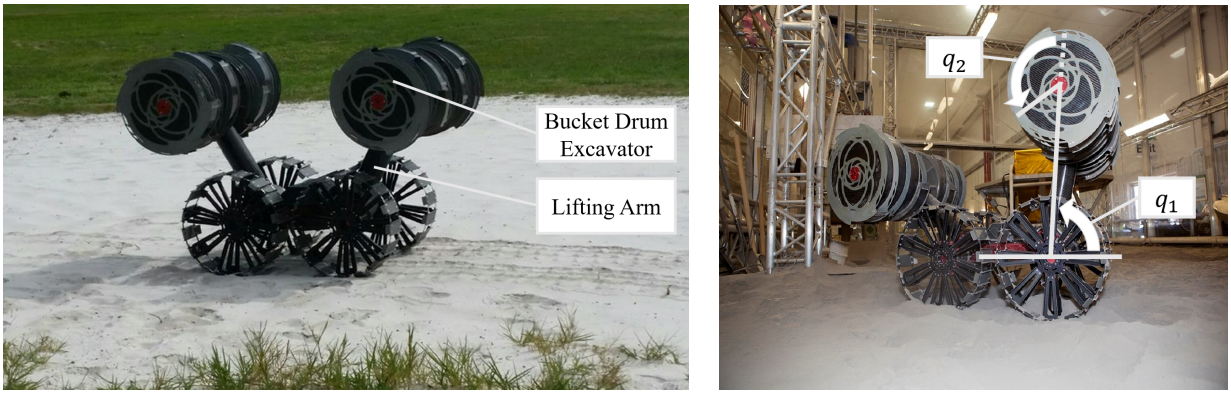

(a) (b)

Figure 1. Labeled pictures of the RASSOR excavation robot. Image (a) identifies the lifting arm and bucket drum excavator of RASSOR, and image (b) illustrates the angular positions q_1 and q_2 of RASSOR.

be exactly determined. The lifting arm and excavator are tasked with following an arbitrary post-excavation desired trajectory while simultaneously identifying the uncertain parameters, and hence, the mass of the excavated material.

Parameter convergence has long been a focus of research in adaptive control.[3–6] Indirect adaptive control laws compensate for the parametric uncertainty in dynamic models by estimating the values of the unknown parameters online. Conventional adaptive control techniques result in a tracking error that asymptotically converges, but the parameter estimate error can only be proven to be bounded.[7] Generally, simultaneous parameter identification only occurs if the persistence of excitation (PE) condition on the regression matrix is met.[7–12] For general nonlinear systems, it is impossible to guarantee the PE condition a priori.[13] Historically, ad hoc methods, such as injecting additive disturbances, which can potentially affect system performance or stability, have been used with the assumption of satisfying the PE assumption. However, in recent years, several alternatives to the traditional PE condition have been developed. One approach is initial excitation (IE).[14,15] IE, unlike PE, assumes the regression matrix is sufficiently excited only in the initial time window and can be verified online. In IE, excitation need not persist as time advances, eliminating the idea of persistence and guaranteeing exponential convergence of the parameter estimate and tracking errors. Another approach is concurrent learning (CL).[16–18] Likewise, CL-based methods rely on a milder excitation condition that can be verified online. Unlike PE or IE approaches, CL uses input-output data pairs of the dynamic system to update the estimated parameters. However, in CL-based methods, the derivative of the highest-order state must be calculated (often numerically). A variation of CL, called integral concurrent learning (ICL), reformulates the traditional CL method by removing the need to take the highest order derivative and related filtering.[13,19]

ICL exploits partial knowledge of the dynamics to achieve exponential convergence of the tracking and parameter errors once sufficient excitation has been obtained. In this paper, a globally exponentially stable tracking controller and ICL-based parameter estimate update law is developed for RASSOR. Once sufficient (finite) excitation is achieved, a Lyapunov-based analysis proves that the tracking and parameter estimate errors converge to zero exponentially. Leveraging estimates of the dynamical system's parameters, the mass of excavated material is estimated. Simulation results demonstrate the feasibility of this method for estimating the mass of excavated material.

II. Robot Dynamics

For the following definitions, $m_1 \in \mathbb{R}$ is the known mass of RASSOR's lifting arm, $m_{ex} \in \mathbb{R}$ is the known mass of the bucket drum excavator, $m_{reg} \in \mathbb{R}$ is the unknown mass of the regolith, $m_2 \triangleq m_{ex} + m_{reg}$ is the unknown combined mass of the bucket drum excavator and regolith, $a_1 \in \mathbb{R}$ is the known length of the lifting arm, $a_2 \in \mathbb{R}$ is the unknown distance from the geometric center of the bucket drum excavator to the combined center of mass of the bucket drum excavator and regolith, and $g \in \mathbb{R}$ is the known magnitude of the local gravity vector. Consider the Euler-Lagrange dynamics of RASSOR's lifting mechanism as

$$M\left(q\left(t\right)\right)\ddot{q}\left(t\right)+V_m\left(q\left(t\right),\dot{q}\left(t\right)\right)\dot{q}\left(t\right)+G\left(q\left(t\right)\right)+F_v\dot{q}\left(t\right)+F_s\left(\dot{q}\left(t\right)\right)=\tau\left(t\right), \tag{1}$$

where $q\left(t\right)\triangleq\left[q_1\left(t\right),\,q_2\left(t\right)\right]^T\in\mathbb{R}^2$ denotes the angle of the lifting arm and the angle of the bucket drum excavator, respectively (see Figure 1), and $\dot{q}\left(t\right),\,\ddot{q}\left(t\right)\in\mathbb{R}^2$ represent the angular velocity and acceleration vectors, respectively. In (1), $M:\mathbb{R}^2\rightarrow\mathbb{R}^{2\times2}$ represents the inertia matrix defined as

$$M\left(q\left(t\right)\right)\triangleq\begin{bmatrix}p_1+2p_3\cos\left(q_2\left(t\right)\right) & p_2+p_3\cos\left(q_2\left(t\right)\right)\\ p_2+p_3\cos\left(q_2\left(t\right)\right) & p_2\end{bmatrix}, \tag{2}$$

where $p_1\triangleq\left(m_1+m_2\right)a_1^2+m_2a_2^2$, $p_2\triangleq m_2a_2^2$, and $p_3\triangleq m_2a_1a_2$ are constant, unknown parameters, $V_m:\mathbb{R}^2\times\mathbb{R}^2\rightarrow\mathbb{R}^{2\times2}$ represents the centripetal-Coriolis effects defined as

$$V_m\left(q\left(t\right),\dot{q}\left(t\right)\right)\triangleq\begin{bmatrix}-p_3\sin\left(q_2\left(t\right)\right)\dot{q}_2\left(t\right) & -p_3\sin\left(q_2\left(t\right)\right)\left(\dot{q}_1\left(t\right)+\dot{q}_2\left(t\right)\right)\\ p_3\sin\left(q_2\left(t\right)\right)\dot{q}_1\left(t\right) & 0\end{bmatrix}, \tag{3}$$

$G:\mathbb{R}^2\rightarrow\mathbb{R}^2$ represents gravitational effects defined as

$$G\left(q\left(t\right)\right)\triangleq\begin{bmatrix}G_1\cos\left(q_1\left(t\right)\right)+G_2\cos\left(q_1\left(t\right)+q_2\left(t\right)\right)\\ G_2\cos\left(q_1\left(t\right)+q_2\left(t\right)\right)\end{bmatrix}, \tag{4}$$

where $G_1\triangleq\left(m_1+m_2\right)ga_1$ and $G_2\triangleq m_2ga_2$ are constant, unknown parameters, $F_v\in\mathbb{R}^{2\times2}$ represents viscous friction effects defined as

$$F_v\triangleq\begin{bmatrix}f_{v1} & 0\\ 0 & f_{v2}\end{bmatrix}, \tag{5}$$

where $f_{v1},\,f_{v2}\in\mathbb{R}$ are constant, unknown viscous friction coefficients, $F_s:\mathbb{R}^2\rightarrow\mathbb{R}^2$ represents static friction effects defined as

$$F_s\left(\dot{q}\left(t\right)\right)\triangleq\begin{bmatrix}f_{s1}\mathrm{sgn}\left(\dot{q}_1\left(t\right)\right)\\ f_{s2}\mathrm{sgn}\left(\dot{q}_2\left(t\right)\right)\end{bmatrix}, \tag{6}$$

where $f_{s1},\,f_{s2}\in\mathbb{R}$ are constant, unknown static friction coefficients, and $\tau\left(t\right):\mathbb{R}_{\geq0}\rightarrow\mathbb{R}^2$ represents the control inputs. The dynamics in (1) have the following properties.

Property 1: The system in (1) is linearly parameterizable. The left-hand side of (1) can be written as

$$Y_1\left(q\left(t\right),\dot{q}\left(t\right),\ddot{q}\left(t\right)\right)\theta=M\left(q\left(t\right)\right)\ddot{q}\left(t\right)+V_m\left(q\left(t\right),\dot{q}\left(t\right)\right)\dot{q}\left(t\right)+G\left(q\left(t\right)\right)+F_v\dot{q}\left(t\right)+F_s\left(\dot{q}\left(t\right)\right), \tag{7}$$

where $Y_1:\mathbb{R}^2\times\mathbb{R}^2\times\mathbb{R}^2\rightarrow\mathbb{R}^{2\times9}$ denotes a regression matrix, and $\theta\in\mathbb{R}^9$ is a vector of constant unknown parameters, defined as $\theta\triangleq\left[p_1,p_2,p_3,G_1,G_2,f_{v1},f_{v2},f_{s1},f_{s2}\right]^T$.

Property 2: The inertia matrix is symmetric, positive definite, and satisfies the following inequalities:

$$I_1\left\|\xi\right\|^2\leq\xi^TM\left(q\left(t\right)\right)\xi\leq I_2\left\|\xi\right\|^2,\,\forall\xi\in\mathbb{R}^2, \tag{8}$$

where I_1 and I_2 are known, scalar constants and $\left\|\cdot\right\|$ represents the Euclidean norm operator.

Property 3: The inertia and centripetal-Coriolis matrices satisfy the following skew-symmetric relationship:

$$\xi^T \left(\frac{1}{2} \dot{M} \left(q \left(t \right) \right) - V_m \left(q \left(t \right), \dot{q} \left(t \right) \right) \right) \xi = 0, \, \forall \xi \in \mathbb{R}^2, \tag{9}$$

where $\dot{M} \left(q \left(t \right) \right) \triangleq \frac{d}{dt} M \left(q \left(t \right) \right)$ is the time-derivative of the inertia matrix.

Post-excavation, the objective is for the lifting arm to follow an arbitrary sufficiently smooth desired trajectory $q_d : \mathbb{R}_{\geq 0} \to \mathbb{R}^2$ while simultaneously identifying the unknown parameters, which can then be used to identify the regolith mass.[a] To quantify the control objective, the tracking error $e : \mathbb{R}_{\geq 0} \to \mathbb{R}^2$ is defined as

$$e \left(t \right) \triangleq q_d \left(t \right) - q \left(t \right). \tag{10}$$

To facilitate the subsequent control design and stability analysis, and proportional derivative-type auxiliary tracking error, denoted by $r : \mathbb{R}_{\geq 0} \to \mathbb{R}^2$, is defined as

$$r \left(t \right) \triangleq \dot{e} \left(t \right) + \alpha e \left(t \right), \tag{11}$$

where $\alpha \in \mathbb{R}_{>0}$ is a constant user-defined gain. The open-loop error dynamics are obtained by taking the time derivative of (11), premultiplying the resulting expression by $M(q\left(t \right))$, and then substituting (1) for $M(q\left(t \right))\ddot{q}\left(t \right)$ to obtain

$$M \left(q \left(t \right) \right) \dot{r} \left(t \right) = M \left(q \left(t \right) \right) \ddot{q}_d \left(t \right) - \tau \left(t \right) + V_m \left(q \left(t \right), \dot{q} \left(t \right) \right) \dot{q} \left(t \right) + G \left(q \left(t \right) \right) + F_v \dot{q} \left(t \right) + F_s \left(\dot{q} \left(t \right) \right) + \alpha M \left(q \left(t \right) \right) \dot{e} \left(t \right). \tag{12}$$

By using Property 1 and (11), (12) can be rewritten as

$$M \left(q \left(t \right) \right) \dot{r} \left(t \right) = Y_2 \left(q \left(t \right), \dot{q} \left(t \right), t \right) \theta - V_m \left(q \left(t \right), \dot{q} \left(t \right) \right) r \left(t \right) - \tau \left(t \right), \tag{13}$$

where the linear parameterization $Y_2 \left(q \left(t \right), \dot{q} \left(t \right), t \right) \theta$ is defined as

$$Y_2 \left(q \left(t \right), \dot{q} \left(t \right), t \right) \theta \triangleq M \left(q \left(t \right) \right) \left(\ddot{q}_d \left(t \right) + \alpha \dot{e} \left(t \right) \right) + V_m \left(q \left(t \right), \dot{q} \left(t \right) \right) \left(\dot{q}_d \left(t \right) + \alpha e \left(t \right) \right) + G \left(q \left(t \right) \right) + F_v \dot{q} \left(t \right) + F_s \left(\dot{q} \left(t \right) \right), \tag{14}$$

where $Y_2 : \mathbb{R}^2 \times \mathbb{R}^2 \times \mathbb{R}_{\geq 0} \to \mathbb{R}^{2 \times 9}$ and θ is defined in Property 1. Based on the open-loop error system in (14) and the subsequent stability analysis, the controller is designed as

$$\tau \left(t \right) = Y_2 \left(q \left(t \right), \dot{q} \left(t \right), t \right) \hat{\theta} \left(t \right) + e \left(t \right) + k r \left(t \right), \tag{15}$$

where $k \in \mathbb{R}_{>0}$ is a constant user-defined gain, and $\hat{\theta} \in \mathbb{R}^9$ is the parameter estimate of θ.

To quantify the parameter identification objective, the parameter estimation error $\tilde{\theta} \in \mathbb{R}^m$ is defined as

$$\tilde{\theta} \left(t \right) \triangleq \theta - \hat{\theta} \left(t \right). \tag{16}$$

A dual objective is completed by identifying θ. Determining θ provides a more accurate feedforward term $(Y_2 \left(q \left(t \right), \dot{q} \left(t \right), t \right) \hat{\theta} \left(t \right))$ in (15) that improves tracking performance, and the mass of excavated regolith can be determined from the definitions of unknown parameter values θ. The definitions of p_1, p_2, p_3, G_1, and G_2 form a system of equations. Solving this system of equations yields an expression for m_2 in terms of unknown parameters and known constants. By using the parameter estimates and by substracting m_{reg} from m_2, the mass estimate of regolith excavated is

[a] Different trajectories could be designed with different frequency characteristics that would lead to sufficient excitation at different timescales.

$$\hat{m}_{reg}(t) \triangleq \frac{\hat{G}_2^2(t)}{\hat{p}_2(t) g^2} - m_{ex}, \tag{17}$$

where $\hat{p}_2(t)$ and $\hat{G}_2(t)$ are elements of $\hat{\theta}(t)$ and g and m_{ex} are known constants.[b]

Remark 1. The system of equations formed by p_1, p_2, p_3, G_1, and G_2 are not independent, hence (17) requires knowledge of the gravitational constant g. Measurement of the gravitational constant on the surface of celestial bodies is a topic of ongoing research. NASA's Gravity Recovery and Interior Laboratory, for example, provides a high-quality gravitational field mapping of the Lunar surface.[20–23]

III. Integral Concurrent Learning

Motivated by the parameter identification objective and to circumvent the need to numerically estimate $\ddot{q}(t)$, an ICL-based adaptation policy is used. Integrating both sides of the dynamics in (1) from $t - \Delta t$ to t yields

$$\mathcal{Y}(q(t), \dot{q}(t), \ddot{q}(t), t)\,\theta = \mathcal{T}(t), \tag{18}$$

where $\mathcal{Y} : \mathbb{R}_{\geq 0} \to \mathbb{R}^{2\times 9}$ and $\mathcal{T} : \mathbb{R}_{\geq 0} \to \mathbb{R}^2$ are defined as

$$\mathcal{Y}(q(t), \dot{q}(t), \ddot{q}(t), t) \triangleq \begin{cases} 0_{2\times 9} & t \in [0, \Delta t], \\ \int_{t-\Delta t}^{t} Y_1(q(\sigma), \dot{q}(\sigma), \ddot{q}(\sigma))\, d\sigma & t > \Delta t, \end{cases} \tag{19}$$

$$\mathcal{T}(t) \triangleq \begin{cases} 0_2 & t \in [0, \Delta t], \\ \int_{t-\Delta t}^{t} \tau(\sigma) & t > \Delta t. \end{cases} \tag{20}$$

To implement (19) without requiring $\ddot{q}(t)$, the term $M(q(t))\,\ddot{q}(t)$ is integrated by parts. Specifically,

$$\int_{t-\Delta t}^{t} M(q(\sigma))\,\ddot{q}(\sigma)\, d\sigma = M(q(t))\,\dot{q}(t) - M(q(t-\Delta t))\,\dot{q}(t-\Delta t) - \int_{t-\Delta t}^{t} \dot{M}(q(t))\,\dot{q}(t). \tag{21}$$

Based on (21) the integral $\int_{t-\Delta t}^{t} Y_1(q(\sigma), \dot{q}(\sigma))\, d\sigma$ can be rewritten as

$$\int_{t-\Delta t}^{t} Y_1(q(\sigma), \dot{q}(\sigma), \ddot{q}(\sigma))\, d\sigma = Y_3(q(t), \dot{q}(t), q(t-\Delta t), \dot{q}(t-\Delta t)) + \int_{t-\Delta t}^{t} Y_4(q(\sigma), \dot{q}(\sigma))\, d\sigma, \tag{22}$$

where the parameterization $Y_3(q(t), \dot{q}(t), q(t-\Delta t), \dot{q}(t-\Delta t))\,\theta$ is defined as

$$Y_3(q(t), \dot{q}(t), q(t-\Delta t), \dot{q}(t-\Delta t))\,\theta \triangleq M(q(t))\,\dot{q}(t) - M(q(t-\Delta t))\,\dot{q}(t-\Delta t), \tag{23}$$

where $Y_3 : R^2 \times R^2 \times R^2 \times R^2 \to R^{2\times 9}$, and the parameterization $Y_4(q(t), \dot{q}(t))\,\theta$ is defined as

$$Y_4(q(t), \dot{q}(t))\,\theta \triangleq -\dot{M}(q(t))\,\dot{q}(t) + V_m(q(t), \dot{q}(t))\,\dot{q}(t) + G(q(t)) + F_v\dot{q}(t) + F_s(\dot{q}(t)), \tag{24}$$

where $Y_4 : R^2 \times R^2 \to R^{2\times 9}$, and θ is defined in Property 1. Therefore, (19) can be rewritten in the implementable form

[b] There are various methods to compute $\hat{m}_{reg}(t)$. Other methods use measurements of m_1 and a_1 in addition to m_{ex} and g. Of all of these methods, (17) uses the fewest number of measurements to compute $\hat{m}_{reg}(t)$.

$$\mathcal{Y}(q(t),\dot{q}(t),t) \triangleq \begin{cases} 0_{2\times 9} & t \in [0,\Delta t], \\ Y_3(q(t),\dot{q}(t),q(t-\Delta t),\dot{q}(t-\Delta t)) + \int_{t-\Delta t}^{t} Y_4(q(\sigma),\dot{q}(\sigma))\,d\sigma & t > \Delta t. \end{cases} \tag{25}$$

The ICL-based adaptive update law for the parameter estimates is[13,19]

$$\dot{\hat{\theta}}(t) = \Gamma Y_2(q(t),\dot{q}(t),t)^T r(t) + \Gamma k_{icl} \sum_{i=1}^{N} \mathcal{Y}_i^T \left(\mathcal{T}_i - \mathcal{Y}_i \hat{\theta}(t)\right), \tag{26}$$

where $k_{icl} \in \mathbb{R}_{>0}$ is a user-defined gain, $\Gamma \in \mathbb{R}^{9\times 9}$ is a user-defined, positive definite gain matrix, $t_i \in [0,t]$ are time points between the initial time and the current time, $\mathcal{Y}_i \triangleq \mathcal{Y}(q(t_i),\dot{q}(t_i),t_i)$, and $\mathcal{T}_i \triangleq \mathcal{T}(t_i)$. Using the relationship in (18), a non-implementable form of the adaptive update law, which is equivalent to (26), can be rewritten as

$$\dot{\hat{\theta}} = -\Gamma Y_2(q(t),\dot{q}(t),t)^T r(t) - \Gamma k_{icl} \left[\sum_{i=1}^{N} \mathcal{Y}_i^T \mathcal{Y}_i\right] \tilde{\theta}(t), \tag{27}$$

which will be used in the subsequent analysis.

IV. Stability Analysis

In this section two Lyapunov-based analyses will be presented to show exponential stability of the tracking and parameter estimation errors. Theorem 1 and its associated proof show that the tracking error $e(t)$ and the parameter estimates $\hat{\theta}(t)$ are bounded, that the system is globally asymptotically stable, and how much the magnitude of the states decay before sufficient excitation is achieved. Theorem 2 and its associated proof leverage the result of Theorem 1 to show that the system is globally exponentially stable starting from $t = 0$ if sufficient excitation is achieved. Assumption 1 mathematically defines the sufficient excitation that must occur to yield an exponential result.

In the following analysis, the operators $\lambda_{\min}\{\cdot\}$ and $\lambda_{\max}\{\cdot\}$ are defined as the minimum and maximum eigenvalue of the argument, respectively.

Assumption 1: The system is sufficiently excited over a finite duration of time (i.e., the finite excitation condition). Specifically, $\exists \underline{\lambda} > 0$, $\exists T > \Delta t : \forall t \geq T$, and $\lambda_{\min}\left\{\sum_{i=1}^{N} \mathcal{Y}_i^T \mathcal{Y}_i\right\} \geq \underline{\lambda}$, where T is the time at which the finite excitation condition is met.[c]

Theorem 1. *For the system defined in (1), the controller in (15) and adaptive update law defined in (26) ensure bounded tracking and parameter estimation error before the finite excitation condition is met.*

Proof. Define a radially unbounded candidate Lyapunov function $V : \mathbb{R}^{13} \to \mathbb{R}_{\geq 0}$ as

$$V(\eta(t)) = \frac{1}{2} r(t)^T M(q(t)) r(t) + \frac{1}{2} e(t)^T e(t) + \frac{1}{2} \tilde{\theta}(t)^T \Gamma^{-1} \tilde{\theta}(t), \tag{28}$$

where $\eta(t) \triangleq \begin{bmatrix} e(t)^T & r(t)^T & \tilde{\theta}(t)^T \end{bmatrix}^T \in \mathbb{R}^{13}$ is a composite state vector. Note that $\beta_1 \|\eta(t)\|^2 \leq V(\eta(t)) \leq \beta_2 \|\eta(t)\|^2$, where $\beta_1 \triangleq \frac{1}{2}\min\left\{m_1, 1, \lambda_{\min}\left\{\Gamma^{-1}\right\}\right\}$ and $\beta_2 \triangleq \frac{1}{2}\max\left\{m_2, 1, \lambda_{\max}\left\{\Gamma^{-1}\right\}\right\}$. Taking the time derivative of (28) and substituting (11), (13), and (27) yields the following upper bound

$$\dot{V}(\eta(t)) \leq -\alpha \|e(t)\|^2 - k \|r(t)\|^2 - k_{icl} \left[\sum_{i=1}^{N} \mathcal{Y}_i^T \mathcal{Y}_i\right] \left\|\tilde{\theta}(t)\right\|^2. \tag{29}$$

[c] Time T is unknown a priori. Since $\lambda_{\min}\left\{\sum_{i=1}^{N} \mathcal{Y}_i^T \mathcal{Y}_i\right\}$ can be calculated online, then time T can also be determined online.

Before the finite excitation condition is reached, $\sum_{i=1}^{N} \mathcal{Y}_i^T \mathcal{Y}_i$ is only positive semi-definite (i.e., $\sum_{i=1}^{N} \mathcal{Y}_i^T \mathcal{Y}_i \geq 0$). Therefore, before finite excitation is achieved, (29) is upper bounded by

$$\dot{V}(\eta(t)) \leq -\alpha \|e(t)\|^2 - k \|r(t)\|^2. \tag{30}$$

Based on Theorem 8.4,[24] $\eta(t) \in \mathcal{L}_\infty$. Hence, $e(t), r(t), \tilde{\theta}(t) \in \mathcal{L}_\infty$. Since $\dot{V}(\eta(t)) \leq 0$, then $V(\eta(T)) \leq V(\eta(0))$, hence

$$\|\eta(T)\| \leq \sqrt{\frac{\beta_2}{\beta_1}} \|\eta(0)\|. \tag{31}$$

Since $\eta(t) \in \mathcal{L}_\infty$ is bounded, integrating (30) indicates that $r(t), e(t) \in \mathcal{L}_2$. Since $r(t), e(t), \hat{\theta}(t) \in \mathcal{L}_\infty$, then $\tau(t) \in \mathcal{L}_\infty$. Invoking Barbalat's Lemma, global asymptotic tracking is achieved in the sense that $\lim_{t\to\infty} r \to 0$ and $\lim_{t\to\infty} e \to 0$.[10] □

Theorem 2 and its associated proof leverage the result of Theorem 1 to show that the system achieves global exponential tracking starting from $t = 0$ if the sufficient excitation is achieved at $t = T$.

Theorem 2. *Provided that Assumption 1 is satisfied, for the system defined in (1), the controller in (15) and adaptive update law defined in (26) ensure global exponential tracking in the sense that*

$$\|\eta(t)\| \leq \frac{\beta_2}{\beta_1} \exp(\lambda_1 T) \|\eta(0)\| \exp(-\lambda_1 t), \tag{32}$$

where $\lambda_1 = \frac{\min\left\{\alpha, k, k_{icl}\lambda_{\min}\left\{\sum_{i=1}^{N} \mathcal{Y}_i^T \mathcal{Y}_i\right\}\right\}}{2\beta_2}$.

Proof. By taking the same steps as in the proof of Theorem 1, (29) is obtained again. Provided that Assumption 1 is satisfied, $\dot{V}(\eta(t))$ is bounded from above as

$$\dot{V}(\eta(t)) \leq -\alpha \|e(t)\|^2 - k \|r(t)\|^2 - k_{icl}\lambda_{\min}\left\{\sum_{i=1}^{N} \mathcal{Y}_i^T \mathcal{Y}_i\right\} \left\|\tilde{\theta}(t)\right\|^2 \ \forall t \in [T, \infty). \tag{33}$$

Substituting (28) into (33) yields

$$\dot{V}(\eta(t)) \leq -\frac{\min\left\{\alpha, k, k_{icl}\lambda_{\min}\left\{\sum_{i=1}^{N-1} \mathcal{Y}_i^T \mathcal{Y}_i\right\}\right\}}{\beta_2} V(\eta(t)) \ \forall t \in [T, \infty), \tag{34}$$

Invoking Theorem 4.10,[24] $\eta(t)$ is globally exponentially stable $\forall t \in [T, \infty)$,

$$\|\eta(t)\| \leq \sqrt{\frac{\beta_2}{\beta_1}} \|\eta(T)\| \exp(-\lambda_1 (t - T)) \ \forall t \in [T, \infty). \tag{35}$$

Combining (31) and (35) yields the result in (32). Since $\eta(t)$ converges to zero exponentially, hence $e(t)$, $r(t)$, and $\tilde{\theta}(t)$ converge to zero exponentially. □

V. Simulation

A simulation was performed to show the efficacy of the developed technique. In this simulation, 3 kilograms of regolith is inside of the bucket drum excavator, which has a known mass of 5 kilograms. The initial conditions of the dynamics are $q(0) = \left[\frac{\sqrt{2}\pi}{2}, -\frac{(1+\sqrt{2})\pi}{2}\right]^T$ and $\dot{q}(0) = [0,0]^T$. The desired trajectory was selected as $q_d(t) = \left[1 + 0.1\cos(t), -\frac{\pi}{2} - (1 + 0.1\cos(t)) + 0.1\cos(0.3t)\right]^T$. The desired trajectory for $q_1(t)$ oscillates between 52° and 63° to avoid contact with the ground. The desired trajectory for $q_2(t)$ is designed to minimize the regolith's motion by keeping the center of mass directly underneath the center of the bucket drum excavator (oscillates within ±5.5° of vertical). The angular position of the excavator arm and drum bucket oscillate with a period of 6 seconds and 21 seconds, respectively. These trajectories correspond to small angular velocities to avoid moving the regolith. The parameters used in the simulation are presented in Table 1. The history stack stops learning after the minimum eigenvalue of the history stack $\lambda_{\min}\left\{\sum_{i=1}^{N} \mathcal{Y}_i^T \mathcal{Y}_i\right\}$ reaches a value of 20. The history stack (i.e., $\sum_{i=1}^{N} \mathcal{Y}_i^T \mathcal{Y}_i$) eventually stops adding data points. At a certain point, adding more data will not increase the convergence rate. By Theorem 1 and 2, the maximum convergence rate is limited by $\min\left\{\alpha, k, k_{icl}\lambda_{\min}\left\{\sum_{i=1}^{N} \mathcal{Y}_i^T \mathcal{Y}_i\right\}\right\}$. In this simulation, once $\lambda_{\min}\left\{\sum_{i=1}^{N} \mathcal{Y}_i^T \mathcal{Y}_i\right\} > 20$, additional input-output data will not increase the rate of exponential convergence. The values selected for m_1, m_{ex}, m_{reg}, a_1, and a_2 correspond to a 3D-printed, 40% scale model of RASSOR. The magnitude of the local gravity vector g corresponds to Lunar gravity.

Table 1. Simulation Parameters

Parameter	Value	Units
m_1	5	kg
m_2	8	kg
m_{ex}	5	kg
m_{reg}	3	kg
a_1	0.3	m
a_2	0.092	m
g	1.65	$\frac{\text{kg}\cdot\text{m}}{\text{s}^2}$
f_{v1}	1.3	-
f_{v2}	1.1	-
f_{s1}	0.2	-
f_{s2}	0.4	-
k	50	-
k_{icl}	0.05	-
α	1	-
Γ	$50 * I_{9\times 9}$	-
Δt	0.2	s

Figure 2 presents the angular tracking error throughout the simulation. The error converges in approximately 5 seconds, which is after parameter convergence occurs. Different control gains may result in different performance.

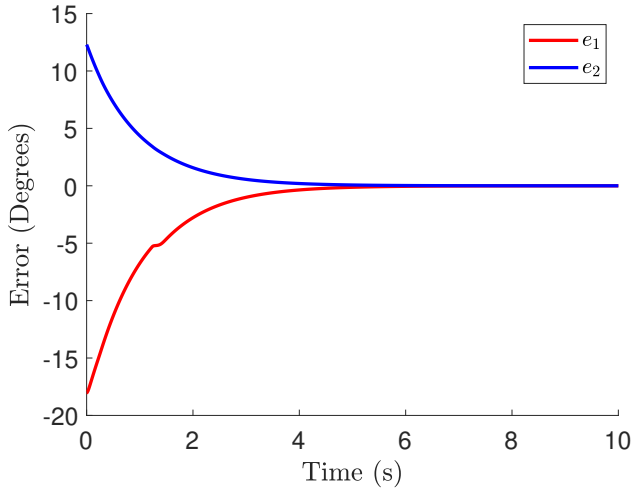

Figure 2. Convergence of the tracking error, $e(t)$.

Figure 3 illustrates the control input in Newton-meters of each motor. While allowable control input is application-specific, these control inputs are within reasonable magnitudes and frequencies.

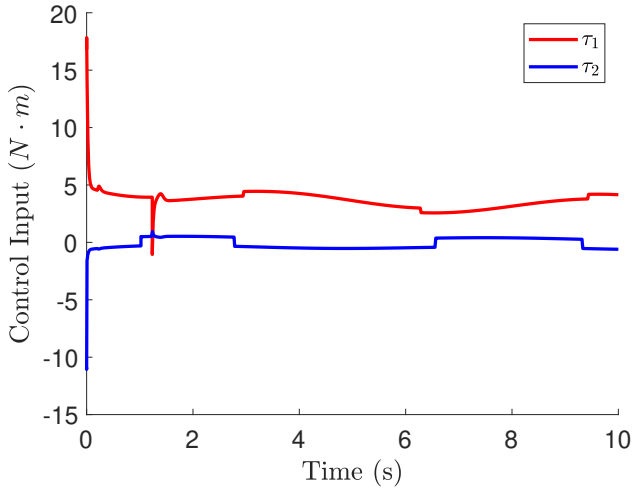

Figure 3. Control input $\tau(t)$ acting at $q_1(t)$ and $q_2(t)$, respectively.

Figure 4 plots the parameter estimates $\hat{\theta}(t)$, compared to their respective actual values θ, and Figure 5 shows the error parameter error $\tilde{\theta}(t)$. After 2 seconds, 3 of the parameters converge to their actual values. The remaining 6 parameters get within a neighborhood of their actual values quickly but converge to their final values more slowly.

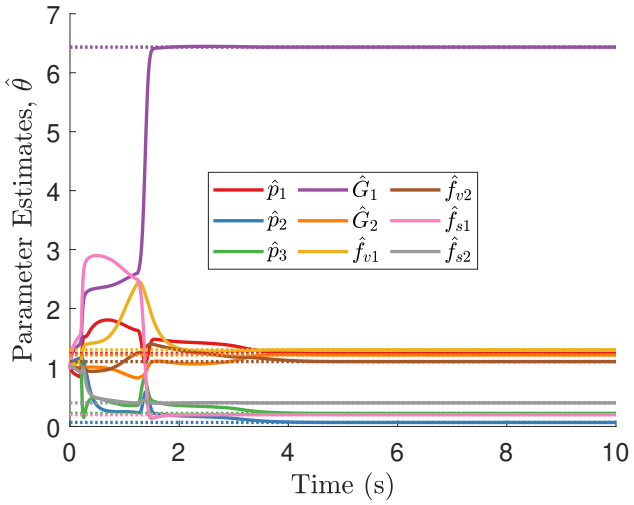

Figure 4. Parameter estimates $\hat{\theta}(t)$ compared to their actual values, θ.

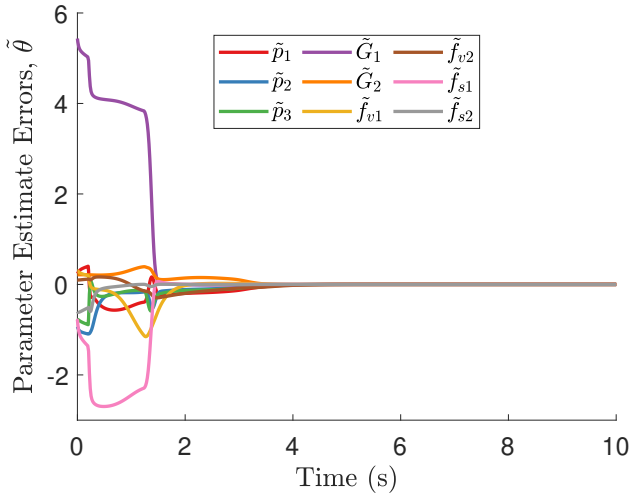

Figure 5. Parameter estimate error $\tilde{\theta}(t)$.

Figure 6 presents the minimum eigenvalue of the history stack $\lambda_{\min}\left\{\sum_{i=1}^{N} \mathcal{Y}_i^T \mathcal{Y}_i\right\}$. Data would not be added to the history stack after $\lambda_{\min}\left\{\sum_{i=1}^{N} \mathcal{Y}_i^T \mathcal{Y}_i\right\}$ reaches a value of 20, though the simulation does not run long enough to reach that threshold.

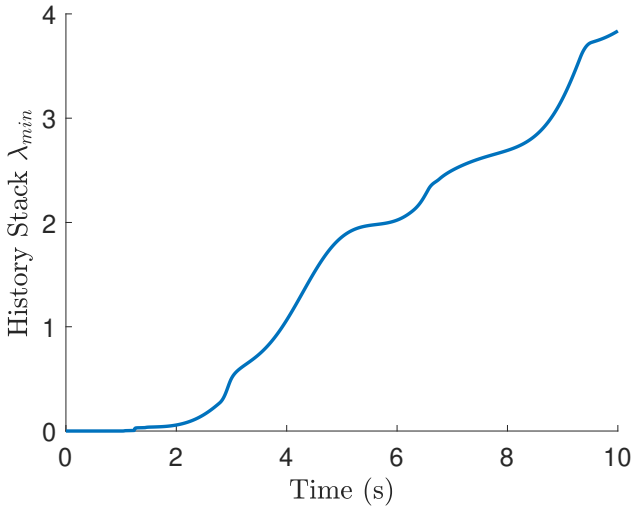

Figure 6. $\lambda_{\min}\left\{\sum_{i=1}^{N} \mathcal{Y}_i^T \mathcal{Y}_i\right\}$, **Minimum Eigenvalue of the History Stack**

Figure 7 shows the estimate of the mass of regolith, calculated from (17). The calculation of $\hat{m}_{reg}(t)$ is sensitive to the quality of the $\hat{p}_2(t)$ and $\hat{G}_2(t)$ estimates. While $\hat{p}_2(t)$ and $\hat{G}_2(t)$ converge near their actual values within 4 seconds, they must converge further to get a better quality estimate of m_{reg}. The root mean square error after 7 seconds is 4.9 grams, or 0.16% error.

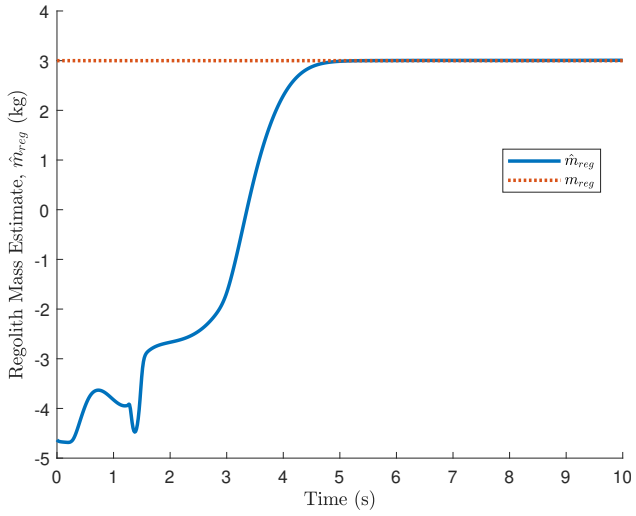

Figure 7. Mass estimate of excavated regolith compared to the actual value.

VI. Conclusion

A Lyapunov-based analysis is used to show that the ICL-based parameter update law and controller enables global exponential tracking of the angular positions of RASSOR's lifting arm and bucket drum excavator ($q_1(t)$ and $q_2(t)$, respectively, as shown in Figure 1) while simultaneously identifying the unknown regolith mass. The ICL-based parameter update law provided exponential convergence of the parameter estimate error while using a finite excitation condition. A simulation was performed that demonstrates that the excavated regolith mass can be estimated from the unknown parameters of the dynamics.

Future works include implementing the developed technique on RASSOR to measure the mass of excavated regolith. These experimental results will be compared with results obtained from calibration-based strategies that correlate motor current with regolith mass. Additionally, motivated by energy constraints, the ICL-based parameter adaptation law could be combined with an approximate dynamic programming-based controller to simultaneously synthesize an optimal control policy and estimate the unknown parameters online.

VII. Acknowledgments

This research is supported by NASA project number 80NSSC20K0711. Any opinions, findings and conclusions or recommendations expressed in this material are those of the author(s) and do not necessarily reflect those of sponsoring agencies.

References

[1]Mueller, R. P., Smith, J. D., Schuler, J. M., Nick, A. J., Gelino, N. J., Leucht, K. W., Townsend, I. I., and Dokos, A. G., "Design of an excavation robot: regolith advanced surface systems operations robot (RASSOR) 2.0," *J. of Aerosp. Eng.*, 2012.

[2]Mueller, R. P., Cox, R. E., Ebert, T., Smith, J. D., Schuler, J. M., and Nick, A. J., "Regolith advanced surface systems operations robot (RASSOR)," *Proc. 2013 IEEE Aerosp. Conf.*.

[3]Boyd, S. and Sastry, S., "Necessary and sufficient conditions for parameter convergence in adaptive control," *Automatica*, Vol. 22, No. 6, 1986, pp. 629–639.

[4]Christoforou, E., "On-line parameter identification and adaptive control of rigid robots using base reaction forces/torques," *Proc. IEEE Int. Conf. Robot. Autom.*, 2007, pp. 4956–4961.

[5]Roy, S. B., Bhasin, S., and Kar, I. N., "Parameter convergence via a novel PI-like composite adaptive controller for uncertain Euler-Lagrange systems," *IEEE Conf. Decis. Control*, Dec. 2016.

[6]Basu Roy, S., Bhasin, S., and Kar, I. N., "Composite Adaptive Control of Uncertain Euler-Lagrange Systems with Parameter Convergence without PE Condition," *Asian J. Control*, 2019.

[7]Slotine, J.-J. E. and Li, W., "On the adaptive control of robot manipulators," *Int. J. Robot. Res.*, Vol. 6, No. 3, 1987, pp. 49–59.

[8]Anderson, B., "Exponential stability of linear equations arising in adaptive identification," *IEEE Trans. Autom. Control*, Vol. 22, No. 1, Feb. 1977, pp. 83–88.

[9]Lewis, F. L., Dawson, D. M., and Abdallah, C., *Robot Manipulator Control Theory and Practice*, CRC, 2003.

[10]Ioannou, P. and Sun, J., *Robust Adaptive Control*, Prentice Hall, 1996.

[11]Narendra, K. and Annaswamy, A., *Stable Adaptive Systems*, Prentice-Hall, Inc., 1989.

[12]Sastry, S. and Bodson, M., *Adaptive Control: Stability, Convergence, and Robustness*, Prentice-Hall, Upper Saddle River, NJ, 1989.

[13]Parikh, A., Kamalapurkar, R., and Dixon, W. E., "Integral Concurrent Learning: Adaptive Control with Parameter Convergence using Finite Excitation," *Int J Adapt Control Signal Process*, Vol. 33, No. 12, Dec. 2019, pp. 1775–1787.

[14]Roy, S. B., Bhasin, S., and Kar, I. N., "Combined MRAC for Unknown MIMO LTI Systems with Parameter Convergence," *IEEE Trans. Autom. Control*, Vol. 63, No. 1, Jan. 2018, pp. 283–290.

[15]Jha, S. K., Roy, S. B., and Bhasin, S., "Initial Excitation-Based Iterative Algorithm for Approximate Optimal Control of Completely Unknown LTI Systems," *IEEE Trans. on Autom. Control*, Vol. 64, No. 12, 2019, pp. 5230–5237.

[16]Chowdhary, G. V. and Johnson, E. N., "Theory and Flight-Test Validation of a Concurrent-Learning Adaptive Controller," *J. Guid. Control Dynam.*, Vol. 34, No. 2, March 2011, pp. 592–607.

[17]Chowdhary, G., Yucelen, T., Mühlegg, M., and Johnson, E. N., "Concurrent learning adaptive control of linear systems with exponentially convergent bounds," *Int. J. Adapt. Control Signal Process.*, Vol. 27, No. 4, 2013, pp. 280–301.

[18]Kamalapurkar, R., Reish, B., Chowdhary, G., and Dixon, W. E., "Concurrent learning for parameter estimation using dynamic state-derivative estimators," *IEEE Trans. Autom. Control*, Vol. 62, No. 7, July 2017, pp. 3594–3601.

[19]Bell, Z., Nezvadovitz, J., Parikh, A., Schwartz, E., and Dixon, W., "Global Exponential Tracking Control for an Autonomous Surface Vessel: An Integral Concurrent Learning Approach," *IEEE J. Ocean Eng.*, Vol. 45, No. 2, April 2020, pp. 362–370.

[20]Zuber, M. T., Smith, D. E., Watkins, M. M., Asmar, S. W., Konopliv, A. S., Lemoine, F. G., Melosh, H. J., Neumann, G. A., Phillips, R. J., Solomon, S. C., et al., "Gravity field of the Moon from the Gravity Recovery and Interior Laboratory (GRAIL) mission," *Science*, Vol. 339, No. 6120, 2013, pp. 668–671.

[21]Wieczorek, M. A., Neumann, G. A., Nimmo, F., Kiefer, W. S., Taylor, G. J., Melosh, H. J., Phillips, R. J., Solomon, S. C., Andrews-Hanna, J. C., Asmar, S. W., et al., "The crust of the Moon as seen by GRAIL," *Science*, Vol. 339, No. 6120, 2013, pp. 671–675.

[22]Lemoine, F. G., Goossens, S., Sabaka, T. J., Nicholas, J. B., Mazarico, E., Rowlands, D. D., Loomis, B. D., Chinn, D. S., Caprette, D. S., Neumann, G. A., et al., "High–degree gravity models from GRAIL primary mission data," *J. of Geophys. Res.: Planets*, Vol. 118, No. 8, 2013, pp. 1676–1698.

[23]Lemoine, F. G., Goossens, S., Sabaka, T. J., Nicholas, J. B., Mazarico, E., Rowlands, D. D., Loomis, B. D., Chinn, D. S., Neumann, G. A., Smith, D. E., et al., "GRGM900C: A degree 900 lunar gravity model from GRAIL primary and extended mission data," *Geophys. Res. Lett.*, Vol. 41, No. 10, 2014, pp. 3382–3389.

[24]Khalil, H. K., *Nonlinear Systems*, Prentice Hall, Upper Saddle River, NJ, 3rd ed., 2002.